TECHNICAL PAPER

Effect of a new type staggered pin fin configuration on flow boiling characteristics of micro-heat sinks

Burak Markal[1] · Beyzanur Kul[2]

Abstract

Flow boiling in micro-pin fin structured heat sinks is an up-to-date thermal management technique. However, due to micro-sized flow passages, bubble blockage is a problem for this type of heat sinks, too. In addition, mixing and bubble breakup are important phenomena for enhancement of heat transfer. Taking more advantages of potential of this unique technique depends on removing of relevant shortcomings and supporting influential mechanisms; therefore, new geometries being designed based on bubble-dynamic characteristics should be developed, and relevant thermo-hydrodynamic characteristics should be analyzed. Therefore, the present paper experimentally analyzes boiling performance of water flow in a micro-pin fin heat sink having a new type of geometry. The heat sink has four sections, and in each section, the micro-fins are positioned in staggered form according to previous sections, also the number of fins in each section is fewer than the one of the former sections. In this paper, for the first time in the literature, combined influence of regional staggered pin fin arrangement and regional cross-sectional enlargement on thermo-hydrodynamic characteristics of flow boiling in micro-pin fin heat sinks is investigated. The new type of heat sink (NT) is compared with conventional type (CT) in which the micro-pin fins are uniformly located throughout the heat sink. Saturated flow boiling experiments are conducted at a heat flux range of 132–272 kW m^{-2} (90 W to 180 W with 10 W increments), and at a constant mass velocity of 174 kg m^{-2} s^{-1} for constant inlet temperature of 75 °C. It is concluded that staggered pin fins with decreasing number significantly boost thermal and flow characteristics. Compared to the conventional type, two-phase heat transfer coefficient increases up to 94.5%, and pressure drop decreases up to 18.3% via NT. The wall superheat for NT is lower than those obtained for CT for the whole database, which physically means that NT keeps the heating surface at lower temperature for the same heat load. Prevention of bubble blockage problem, suppression of flow reversal, enhancement of bubble disjunction, decrease of vapor-waiting time on heat transfer surface, and more effective convective boiling characteristics are the main underlying reasons of performance enhancement.

Keywords Area-based staggered distribution · Visualization · Flow boiling · Microscale

Abbreviations

CT   Conventional micro-pin fin heat sink
NT   Novel type micro-pin fin heat sink

List of symbols

A_{fn} Wetted area of a single fin, m^2
A_{hw} Total heat transfer area, m^2
A_{nf} Area without fins at bottom of channels, m^2

A_{pt} Top platform area of heating piece, m^2
d_L Distance from inlet of the channels to any desired location, m
L_h Heating length, m
q_{hl} Heat loss, W
q_{hp} Heating power, W
T Temperature, K
T_{em} Mean temperature of heat sink, K
W_h Heating width, m

Subscripts

a Ambient
ch   Channel
cl   Constriction
er   Expansion

✉ Burak Markal
burakmarkal@ktu.edu.tr; burakmarkal61@gmail.com

1   Department of Mechanical Engineering, Karadeniz Technical University, 61080 Trabzon, Turkey

2   Department of Energy Systems Engineering, Recep Tayyip Erdogan University, 53100 Rize, Turkey

1 Introduction

Interest to the methods effectively removing heat fluxes from components is increasing day by day. The main underlying reason is reduction in dimensions due to improved machining techniques in addition to increasing functionality; such that, this means huge increments in heat fluxes releasing from heating surfaces. In the literature, as emphasized by Karayiannis and Mahmoud [1], it is supposed that the heat flux released from chips of the computers will reach nearly up to 450 W/cm^2 in the future. To fulfill this demand or need, boiling of a liquid flowing in microchannels is one of the best influential ways since the much higher values of heat transfer coefficients can be achieved during phase-changed convection processes compared to the counterparts. Combination of high compactness, forced flow, and phase-change phenomenon makes flow boiling in microscale passages a popular research area. Therefore, this thermal management technique gets edges over other well-known cooling methods such as vortex tubes [2], jet impingement [3, 4], and heat pipes [5, 6].

Research regarding flow boiling in microchannels basically focuses on understanding of flow nature and/or enhancement of performance characteristics. The weak side for the potential of flow boiling in microchannels is instabilities mainly stemming from bubble-dynamic-based problems such as compressible volume and blockage of the vapor bubbles. Also, improvement of mixing and support of nucleation are two other key factors related to geometry for higher boiling performance. Therefore, geometrical arrangements considering bubble dynamics are the most critical issue for performance enhancement, and thus, up-to-date studies focus on this point.

Lee and Pan [7] experimentally evaluated influence of diverging channel on flow boiling of water. A single microchannel was used. Diverging channel enlarges from the inlet of the channel to the outlet with a constant angle of 0.183° for 25 mm channel length. They concluded that diverging channel was better to suppress the instabilities, and it improved thermal performance compared to uniform channel. A series of similar type studies were conducted by Lu and Pan [8, 9]. In Ref. [8], they experimentally focused on a heat sink having ten diverging parallel channels with the diverging angle of 0.5°. Hydraulic diameter of each channel was 120 μm. Depending on the magnitudes of the inlet temperature and pressure (or pressure drop) results, more stable performance was reported compared to the uniform parallel channels presented in the literature. In their other study [9], same heat sink (hydraulic diameter of 120 μm, 0.5° diverging angle) was compared with the parallel channel heat sinks having diverging channels and artificial nucleation sites (ANSs). It was concluded that the heat sink containing diverging channels with ANSs along each channel performed better thermal performance compared to the heat sink having no ANSs, and the heat sink having ANSs after second half of each channel. However, for all the conditions, the highest value of pressure drop was obtained for the heat sink containing diverging channels with ANSs along each channel. Fu et al. [10, 11] performed experiments with a single silicon channel having diverging angle of 1° and 24 laser-drilled cavities. In Ref. [10], the working fluid was binary mixture of ethanol–water. They reported that molar fraction and mass flux obviously affected boiling characteristics. Increasing mass flux increased critical heat flux (CHF), and optimum thermal performance was obtained for mole fraction of 0.1 (relatively small ethanol content in water). The flow pattern corresponding to highest heat transfer coefficient was reported as bubbly/elongated/slug flow; and convective boiling was addressed as dominant mechanism. On the other hand, in Ref. [11], same authors focused on a visualization-based study. Flow boiling of binary mixtures (methanol/water and ethanol water pairs) and flow pattern maps were in the scope of their study. During boiling process, four distinct regimes were addressed as (1) bubbly/elongated/slug flow, (2) annular flow, (3) breakup of liquid film, and (4) dryout. Based on non-dimensional numbers (Weber, boiling, and Marangoni numbers), a transition criterion between flow regimes was proposed.

For classical microchannels, as stated above, via diverging channel forms, it was shown that thermal performance could increase, and boiling instabilities could decrease. Also, support of nucleation throughout the heat transfer surfaces boosts heat dissipation performance of coolers. However, despite relevant bubble-dynamic-based geometrical modifications performed for conventional parallel channels, much more attention is paid to micro-pin fin type heat sinks in the up-to-date literature. Micro-pin fins can simultaneously provide many advantages which enable performance increase; such that, in the relevant literature, Wan et al. [12] and Deng et al. [13] summarized the merits of micro-pin fin heat sinks: (1) destruction of boundary layer, (2) enhancement of mixing, (3) support of nucleation, (4) increasing of compactness, and (5) prevention of entrapment of growing bubbles in the restricted areas. It should be underlined that above-mentioned five advantages, in deed, correspond to potentials of micro-pin-finned heat sinks, and much more utilization of the relevant potentials can only be achieved via superior geometrical designs. Below, the literature considering micro-pin fins with flow boiling is summarized:

Lie et al. [14] carried out tests for evaluation of thermo-fluidic characteristics of flow boiling of FC-72 in three different heat sink geometries. Regarding geometry, they considered different heat sinks with and without fins. The finned heat sinks had either 200 μm × 200 μm (with 200 μm

distance between fins) or 100 μm × 100 μm (with 100 μm distance between fins) cross-sectional area. Compared to heat flux, effect of mass velocity on two-phase heat transfer coefficient was reported as weak. Bubble departure diameter decreased, nucleation rate increased, and thermal performance was enhanced due to micro-pin fin structure. Regarding the heat sink having larger pin fins, bubbles departed from the surface with a smaller volume. Decreasing cross section of the fin led heat removal capacity to boost. Differently from Ref. [14], Krishnamurthy and Peles [15] focused on staggered pin fin distribution and studied flow boiling. The working fluid was water. The fins of the heat sink were in the shape of circular with diameter of 100 μm and height of 250 μm. In the tests, dominantly, two flow patterns were observed: (1) slug and (2) annular; and a heat transfer coefficient model was developed based on convective boiling. Heat transfer coefficient was not influenced by heat flux, but mass flux positively affected heat transfer coefficient. Ma et al. [16] mainly evaluated influence of fin height on flow boiling of FC-72. They took into consideration two different pin fin heat sinks; one of them had fin height of 60 μm and, and the other one had fin heights of 120 μm. Also, the heat sink having no fins, called as smooth heat sink was used for reference case; and the smooth heat sink was reported to present the poorest cooling performance. Higher fins enhanced heat transfer. Investigation of flow boiling of water in a heat sink having square micro-pin fins (in the form of staggered array) was handled by Qu and Siu-Ho [17] for different operational parameters. Only saturated conditions were taken into consideration, and a correlation for prediction of heat transfer coefficient was proposed. It was reported that influential heat transfer mechanism was convective boiling, which related to annular flow.

Law and Lee [18, 19] conducted two consecutive studies. In the first study [18], compared to parallel channel heat sinks, they obtained superior thermal characteristics with oblique type pin finned heat sink. The flow boiling tests were conducted with FC-72. Heat transfer performance was improved by oblique pin fins; and the reason was attributed to higher bubble population and continuously destroying of liquid film. However, regarding pressure drop, a disadvantage occurred; such that, compared to parallel channel heat sink, pressure drop increased up to 1.7 times. In the other study [19], they experimentally evaluated effect of width of secondary channel (0.45 mm, 0.3 mm, or 0.15 mm). Smaller secondary passages were reported that they were better for thermal performance. Due to decreasing secondary channel width, instabilities could be suppressed more effectively, and CHF was postponed to higher levels. In addition, pressure drop increased with increase in width of secondary channels. Wan et al. [12] conducted experiments to optimize shape of pin fins for flow boiling performance. Staggered configuration was taken into consideration with four different

fin shapes: diamond, circular, square, and streamline. The square fin was the optimum choice for thermal performance, and diamond fin was the poorest one. Despite disadvantage of diamond shape regarding heat transfer, it provided the lowest value of pressure drop. Deng et al. [20] combined micro-pin fin structure with reentrant design, and experimentally analyzed the relevant geometry under different operational conditions including two working fluids (ethanol and water). Heat sink with conventional parallel reentrant channels was used as the conventional geometry for comparison, and heat transfer coefficient increased up to 284% in water tests via novel heat sink compared to conventional one. The underlying reasons were attributed to improvement of nucleation characteristics and reducing of the effect of bubble confinement problem. Increasing heat flux adversely affected heat transfer coefficients.

Chien et al. [21] developed a new fin type called as nucleated fin. The fins having overall dimensions of 100 μm × 100 μm × 100 μm were in the form of Ω-shape-cavities (60 μm pore size with 45 μm opening). The fluid was FC-72. The observed flow patterns were bubbly and slug flow from low to high heat fluxes, respectively. Decreasing saturation temperature led to increase in wall superheat temperature. Qin et al. [22] investigated thermal and flow behavior of water-boiling in hydrophobic coated surfaces with different pin fin shapes (diamond, ellipse, circular, triangle). Diamond shape micro-fins performed the best results since they improved or eased breaking up of the vapor bubbles. Hydrophobic coatings decreased flow resistance; however, despite enhancement in flow characteristics, existence of surface coating and/or increasing hydrophobicity deteriorated thermal performance owing to increasing thermal resistance. Deng et al. [13] manufactured a novel fin shape named as open-ring pin fin, and they experimentally studied thermo-hydrodynamic characteristics of flow boiling of water for both staggered and inline arrays. Type of the fins eased bubble nucleation, and thus, the value of wall superheats corresponding to onset of nucleate boiling (ONB) corresponded to relatively low values as 1–2 °C independent from fin arrangement. However, thermal performance of inline fin arrangement was better than the staggered one; and the lower pressure drops were obtained for inline distribution.

Flow boiling in micro-pin fin structured heat sinks is an up-to-date thermal management technique. To take more advantages of potential of this unique technique, new geometries primary being designed based on bubble dynamic characteristics should be developed, and relevant thermo-hydrodynamic characteristics should be deeply analyzed via high-speed visualization. Despite existence of flow passages at both transverse and forward directions, due to microscaled cross-sectional areas, bubble blockage is an ongoing problem for micro-pin finned

channels, too. This problem should be solved to provide higher thermal performance. In addition, mixing is an important mechanism for enhancement of heat transfer; and design of the fins in staggered form is one of the most effective ways to mix two-phase flow. Staggered layout of fins also enables breakup of the enlarging bubbles. However, regarding micro-pin-finned channels, as seen in literature survey, up to now, only conventional staggered arrangement (the staggered fin pattern comprising the first and second fin-rows continues through the heat sink.) was taken into consideration. To solve these problems and/or to fulfill relevant gaps, and to contribute to the available literature, the goal for the present paper is to experimentally investigate the combined effect of new type staggered arrangement and regional cross-sectional enlargement along the heat sink. For the first time in the literature, combined influence of regional staggered pin fin arrangement and regional cross-sectional enlargement on thermo-hydrodynamic characteristics of flow boiling in micro-pin fin heat sinks is investigated. There are four regions throughout the heat sink; and in each region, the fins are located with staggered arrangement and less number according to the ones in the former region. The underlying mechanisms are evaluated in microscopic scale via high-speed visualization.

2 Experimental apparatus: details, test section, and correlations

2.1 Details of experimental apparatus

The diagram of the experimental apparatus of the present article is shown in Fig. 1, with reference to all equipment. Deionized water was used as the working fluid, and it was filled to a reservoir coupled with a heater after filtering. The heating feature of the reservoir was used in the process of degassing the water before the tests; it is a common practice in boiling tests [23, 24]. Separation of dissolved gas from water before experiments is an important process to eliminate adverse effects of gases on boiling process; such that increasing liquid temperature leads the release of dissolved gases of water during experiments. This process was accomplished by vigorous boiling of water. Then, the control of gas content was provided via a dissolved oxygen meter. The fluid was sucked from the reservoir and pumped into the pipelines via a micro-screw type pump. This pump was controlled with a digital unit. Via the pump driver, flowrate could be easily changed, and the value of flowrate was gained control by a flow meter having digital screen. The pressure in the outlet-line (at pump exit) was measured via a manometer with the aim of control of any possible problems regarding flow continuity. To clearly analyze effect of
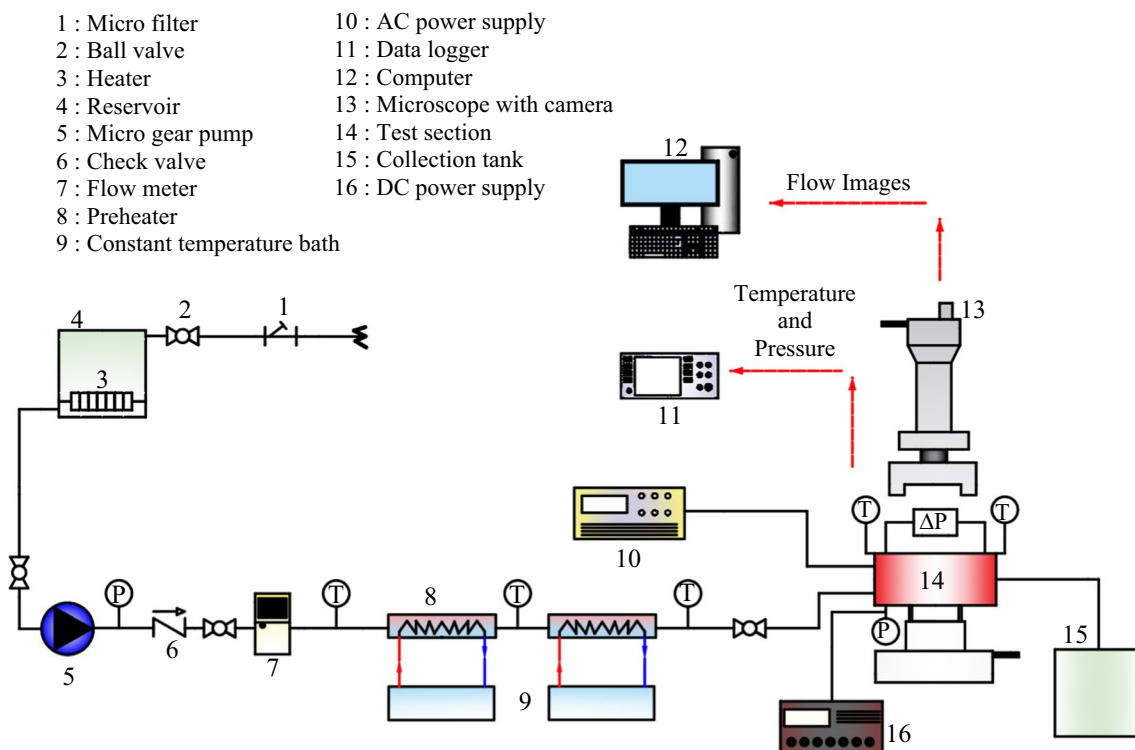
1 : Micro filter
2 : Ball valve
3 : Heater
4 : Reservoir
5 : Micro gear pump
6 : Check valve
7 : Flow meter
8 : Preheater
9 : Constant temperature bath
10 : AC power supply
11 : Data logger
12 : Computer
13 : Microscope with camera
14 : Test section
15 : Collection tank
16 : DC power supply

Fig. 1 Schematic of the experimental apparatus

1: Teflon (PTFE)   6: Channel for thermocouple
2: Inlet chamber   7: Channel for differential pressure sensor
3: Outlet chamber   8: Port for absolute pressure sensor
4: Heating piece   9: Transparent cover
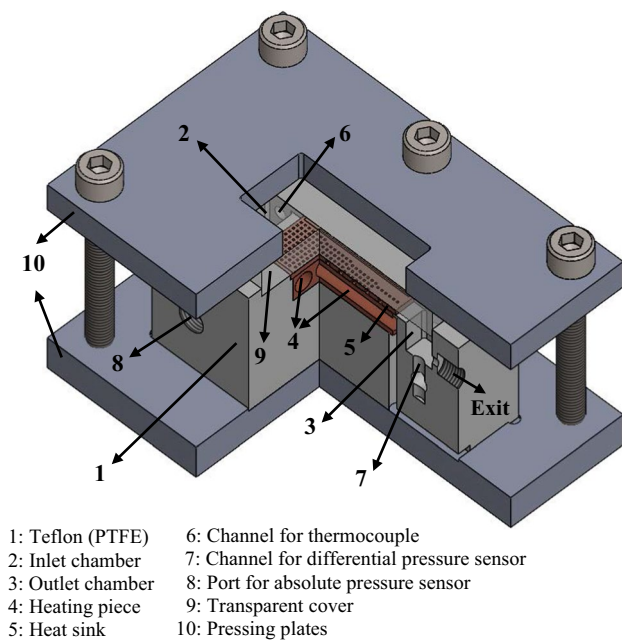5: Heat sink   10: Pressing plates

Fig. 2 Description of test section via sectional view

any parameter, working fluid should enter the heat sink at same/constant temperature; and in this regard, two inline type heaters (heat exchanger + temperature bath) were used to control inlet temperature of water. Temperature baths are highly precision devices with the accuracy of ± 0.02 °C, and used for calibration of the thermocouples, too. After exiting the heaters, water reached to the test section through insulated pipelines.

Test section is presented as sectional view in Fig. 2 to clearly show internal components. Main casing was made of Teflon (polytetrafluoroethylene/PTFE). Main casing is essentially a carrier for other components of the test section and/or measurement devices related to test section. In main casing, along the main flow direction, there are three separate cavities. First of them is the inlet chamber, in which, three connection ports were engraved to measure inlet temperature and pressure, in addition to inlet port. The port related to differential pressure sensor is at the bottom surface of the inlet chamber. The other ports are at the side walls; one of them is for thermocouple (T-type) and the other one is for absolute pressure transducer. The second branch of the differential pressure sensor is connected to the bottom surface of the outlet chamber. The input and output chambers are the same, with one difference: there is one more port in the inlet plenum and this port is for the absolute pressure sensor. It should be noted that both the pressure sensors were connected to a DC power supply. The third cavity is for heating piece made of copper and includes two longitudinal cartridge heaters (each of maximum 120 W). Cartridge heaters were connected to the AC power supply to being

electrically supplied. Heating piece may symbolize a chip of any electronic devices; and therefore, the cooler should be placed over it. In this regard, heat sinks were placed on the heating piece. In up-to-date studies, visualization is quite essential for analysis of background-mechanisms. Therefore, a cover plate enabling to being seen the flow was put on heat sink. Prevention of any liquid leakage is quite important; and therefore, transparent cover should be strongly jammed. To achieve this, two metallic plates were used, and test section was compressed via screw bolts, as seen in Fig. 2.

The most critical pieces of the test section are the heat sinks of which the details are presented in Fig. 3. In Fig. 3a, an isometric solid view of conventional micro-pin fin heat sink is presented. This heat sink was coded with CT; and in the following sections, this abbreviation has been used. In this conventional type, there are 27 rows and 10 columns of micro-pin fins (totally 270 fins). Height of the fins is 200 μm, and they have square cross section as projection (500 μm × 500 μm). Also, the fins are uniformly located throughout the heat sink, and the distance between fins is 1 mm in both transverse and longitudinal direction. The hydraulic diameter of primary and secondary channels is 333 μm. On the other hand, in Fig. 3b, isometric solid view of novel type micro-pin fin heat sink is presented. This heat sink was coded with NT, and in the following sections, this abbreviation has been used. It should be noted that geometric dimensions of the micro-fins are same for both the heat sinks. In the novel heat sink (NT), there are four separate regions. In the first region, there are 7 rows and 10 columns of micro-pin fins. After the first region, a geometrical change occurs; and in this regard, in the second region, there are 7 rows and 9 columns of micro-pin fins. All the fins in the second region are in staggered form according to the first region; and thus, expansion and sectional or regional-based staggering are simultaneously achieved. In the third region, there are 7 rows and 8 columns of micro-pin fins. Similarly, again, both the fins are in staggered form against the former region, and gradual expansion is maintained. In the last region or forth region, there are only 6 rows and 4 columns of fins. In this region, the flow passages between the neighboring fins are also larger than the ones of the other regions; and existing fins are in staggered form compared to the fins in the former region. Therefore, sectional-based expansion and staggered forms are achieved. Other details regarding fin distribution and/or regional differences of NT are presented in Fig. 4.

Except the fin distribution, all the other geometrical properties are same for both heat sinks. In Fig. 3c, thermocouple positions are seen. There are seven thermocouples along the heat sink; however, the generally applied methodology (the most saturated conditions) in the literature [13, 25, 25] was followed; and therefore, in the calculations regarding local two-phase heat transfer coefficient and vapor quality, only
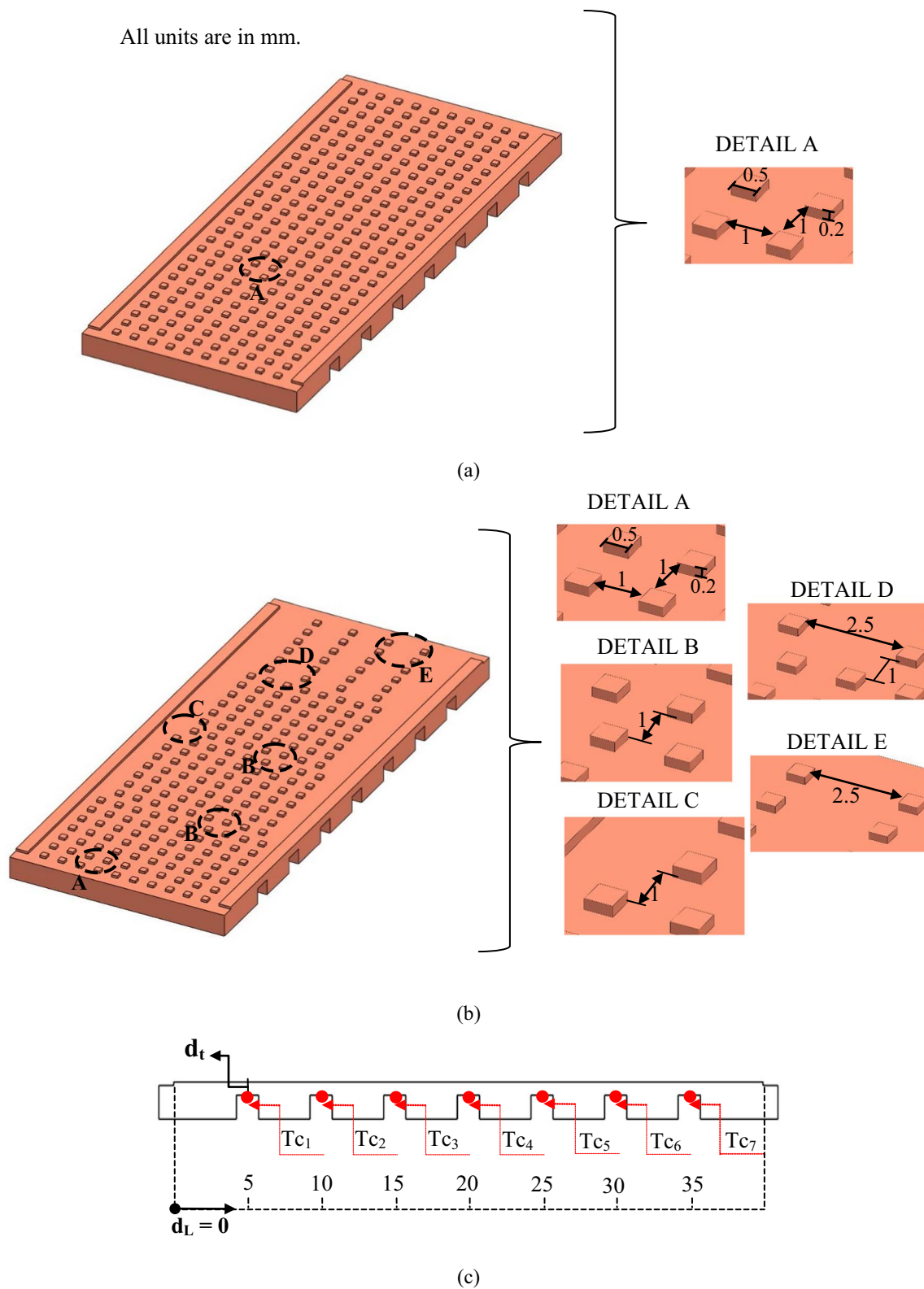
All units are in mm.

DETAIL A

(a)

DETAIL A

DETAIL D

DETAIL B

DETAIL E

DETAIL C

(b)

d_t

Tc_1 Tc_2 Tc_3 Tc_4 Tc_5 Tc_6 Tc_7

5   10   15   20   25   30   35

$d_L = 0$

(c)

Fig. 3 Details of CT (**a**) and NT (**b**), and thermocouple locations for both of them over side view
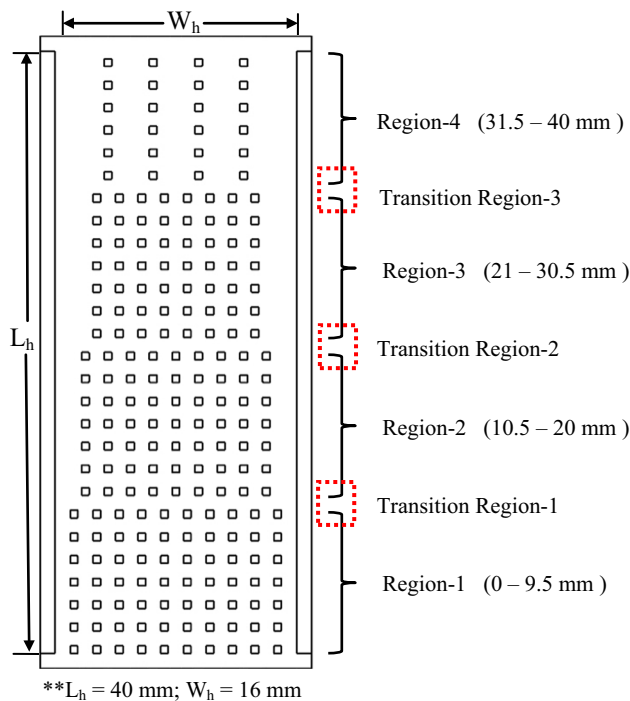
Fig. 4 Detailed demonstration regarding novelty of the NT

the last, in other words, seventh thermocouple was taken into consideration. From Fig. 3c, it is clearly seen that location of seventh thermocouple corresponds to 35 mm from channels' inlet. Thickness of the heat sinks is 2 mm; however, thermocouples were positioned at only 0.5 mm below the channel bottom surface ($d_t = 0.5$ mm; please see Fig. 3c). As stated above, heat sinks were positioned on the heating piece of which platform area is 40 mm × 16 mm (length × width). As compatible with the heating piece, effective heating length (L_h) and width (W_h) of heat sinks (as seen in Fig. 4) are 40 mm and 16 mm, respectively. Overall length and width of the heat sinks are 1 mm longer at each side compared to effective heating dimensions. These excess parts were positioned on Teflon main casing to ensure fluid sealing or prevent fluid leakage. In addition, it should be stated that the heat sinks were manufactured with very precise and quality CNC milling machine. In this regard, the average roughness (Ra) of the heat transfer (channel) surface is approximately 0.09 μm; and it was determined via profilometer. Also, geometrical uncertainty is approximately ± 0.5 μm.

In up-to-date boiling studies, flow visualization has critical importance; and therefore, great attention was paid to visualization. In this regard, a high-quality microscope coupled with high-speed camera was used. The value of frame per second (fps) was adjusted to 1000 for all images; and in addition, for the images, main direction of the flow was from left to right. The measurements were collected through the data-logger.

2.2 Steps performed during a test

Steps performed during a test can be briefly described as follows:

I. Working fluid was degassed by boiling to reduce the oxygen dissolved in the fluid.

II. Circulation of working fluid was initiated by powering the pump. For these test conditions, volumetric flow rate was arranged to 23 ml min^{-1}, which corresponds to nearly $G = 174$ kg m^{-2} s^{-1}.

III. Activation of constant temperature baths was performed. Therefore, the working fluid passing through heat exchangers could be set to be obtained the desired inlet temperature.

IV. The cartridge heaters were powered via an AC power supply. Also, via a DC power supply, pressure sensors were activated.

V. In the tests, heat loads gradually (with 10 W steps) increased between 90 and 180 W (only saturated region was taken into consideration). The heat load of 90 W corresponds to effective heat flux of 132 kW m^{-2}, and the one of 180 W corresponds to 272 kW m^{-2}. At each heat load, at the steady-state conditions, readings were collected.

VI. For any heat sink, above instructions were carried out at each heat load. Then, another heat sink was placed, and the procedure was maintained.

2.3 Evaluation procedure regarding data

To get rid of inlet cross-sectional effect in flow boiling studies regarding microchannels, mass flux, or in other words, mass velocity was used. The equation regarding this term is presented as follow:

$$G = \frac{\dot{V}\rho_f}{A_i} \tag{1}$$

where the volumetric flow rate directly read from the screen of flowmeter was symbolized by $\dot{V}$, and to obtain mass flow-rate, it was multiplied by density of the fluid denoted by ρ_f. Cross-sectional area at the heat sink inlet was represented by A_i. It should be underlined that both the heat sinks were designed to being have same inlet cross section, or in other words, the inlets of both the heat sinks are same. Therefore, in addition to same mass flux, in the present study, experiments regarding both the heat sinks were also carried out at the same mass flow rate.

One of the most efficient operational parameters effecting boiling characteristics is the heating power. In this regard, via the power supply, heating power (q_{hp}) was applied to heat

sinks. A part of heating power was released to the ambient, and it was named as heat loss (q_{h1}). These two heat terms and the top platform area of heating piece (A_{pt}) were made correlated to obtain effective heat flux (q''_{eff}) as in following form:

$$q''_{eff} = \frac{q_{hp} - q_{hl}}{A_{pt}} \quad (2)$$

Width and length of the top/upper platform area of the heating piece is equal to the effective heating width (W_h) and length (L_h) of heat sinks; details are seen in Fig. 4. In this regard, the explicit form of A_{pt} was defined as follows:

$$A_{pt} = W_h \, x \, L_h \quad (3)$$

On the other hand, heat loss was obtained by applying heating power to empty heat sink as commonly followed by researchers in the literature [26]. Test section without any fluid was exposed to heat load, and at steady conditions for each value of heat load, difference of mean temperature of heat sink (T_{em}) and ambient temperature (T_a) were recorded as corresponding to the relevant heat load. Thus, a calibration curve is obtained. As an example, for NT, the calibration curve including relevant correlation was presented in Fig. 5. Same procedure was also performed for CT and taken into consideration in calculation of heat loss. The calibration formulas for CT and NT are also presented as follows:

$$CT : q_{hl} = 0.0687 (T_{em} - T_a) - 0.0523 \quad (4)$$

$$NT : q_{hl} = 0.0683 (T_{em} - T_a) - 0.0319 \quad (5)$$

In this paper, as commonly followed by the other researchers [13], for local value of the two-phase heat transfer coefficient the most downstream location of temperature measurement was taken into consideration due to the higher saturated conditions. It corresponds to 35 mm from the channel inlet.
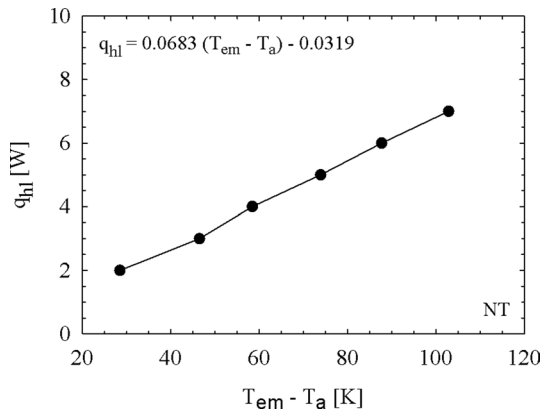

Fig. 5 Curve for heat loss regarding NT

The equation seen below was used to obtain the heat transfer coefficient:

$$h_{tp} = \frac{q_{hp} - q_{hl}}{A_{hw} (T_w - T_{sat})} \quad (6)$$

The whole or total heat transfer area was symbolized with A_{hw}, local wall and saturation temperatures were denoted by T_w and T_{sat}, respectively. It should be emphasized that only saturated conditions were taken into consideration in the present paper. The formula used to obtain T_w is presented below with assumption of 1D heat conduction.

$$T_w = T_{tt} - q''_{eff} \left(\frac{d_t}{k_c} \right) \quad (7)$$

Here T_{tt} denotes temperature value read by the relevant thermocouple. Also, heat sink material is cooper, and its thermal conductivity was represented by k_c. In saturated region, pressure and temperature are function of each other. In this regard, between inlet and outlet pressures, linear interpolation was applied to obtain the local pressure, as compatible with the literature [12, 19]; and corresponding saturation temperature was taken into consideration. The whole or total heat transfer area (A_{hw}) was obtained by considering the finned structure:

$$A_{hw} = A_{nf} + \eta N A_{fn} \quad (8)$$

In the above equation, A_{nf} denotes the area without fins at bottom of channels; and A_{fn} denotes wetted area of a single fin. On the other hand, fin efficiency was represented by η, and fin number was represented by N.

$$A_{fn} = H_{fn} P_{fn} \quad (9)$$

$$A_{nf} = W_h L_h - N A_{fc} \quad (10)$$

For fins, the cross-sectional area was represented by A_{fc} (length of the fin x width of the fin), and cross-sectional perimeter was denoted by P_{fn}. On the other hand, H_{fn} represents fin height. The assumption of adiabatic tip was used in fin analysis. The explicit form of fin efficiency was presented as below:

$$\eta = \frac{tanh(m_{fn} H_{fn})}{m_{fn} H_{fn}} \quad (11)$$

Here m_{fn} represents fin parameter, and it was defined as follows:

$$m_f = \sqrt{\frac{h_{tp} P_{fn}}{k_c A_{fc}}} \quad (12)$$

The above closed formulas could easily be solved to obtain heat transfer coefficient regarding two-phase flow.

Between Eqs. (6, 8–12), an iteration was performed. This procedure was commonly followed in literature [19, 27]. Thermodynamic equilibrium quality (x_e) was calculated via the below equation:

$$x_e = \frac{1}{h_{fg}}\left(\frac{q''_{eff} A_{pt} d_L}{\dot{m} L_h} - c_p \left(T_{sat} - T_{f,in} \right) \right) \qquad (13)$$

Vaporization latent heat was represented by h_{fg}; distance from inlet of the channels to any desired location was represented by d_L; fluid inlet temperature was symbolized with $T_{f,in}$; and specific heat was denoted by c_p.

Microscale flow passages do not provide opportunity to directly measure the local pressure throughout the heat sinks. Therefore, local pressure should be obtained via an alternative way. In this regard, the pressure difference or drop (ΔP) between inlet and outlet plenums was directly measured via the differential pressure sensor. This pressure difference term exactly consists of constriction pressure loss (ΔP_{cl}) between inlet plenum and channel inlet, the channel pressure drop (ΔP_{ch}: pressure loss along the flow passages), and expansion pressure difference (ΔP_{er}) between channel outlet and outlet plenum.

$$\Delta P = \Delta P_{cl} + \Delta P_{ch} + \Delta P_{er} \qquad (14)$$

The expansion pressure difference term (ΔP_{er}) was also named as expansion pressure recovery by Qu and Siu-Ho [17] and Qu and Mudawar [28] due to the dominance of increase in static pressure over expansion losses. As stated in the literature [12, 13], the magnitudes of sudden constriction or expansion pressure differences are negligible compared to channel pressure drop; or their total impact is in the negligible level due to loss and expansion values. Thus, the measured pressure drop can be evaluated as equal to the pressure drop throughout the heat sink ($\Delta P = \Delta P_{ch}$). Also,

although channel pressure drop consists of single and two-phase pressure drop components, single-phase component is negligible compared to two-phase counterpart due to dominant two-phase conditions throughout the flow passages. In other words, pressure drop term (ΔP) may be equal to two-phase pressure drop (ΔP_{tp}).

2.4 Evaluation of uncertainties

Uncertainties should be evaluated over two aspects: (1) measurement-based quantities, and (2) derived parameters. The first group is directly related to the capacities or sensitives of the devices used during experiments; and the relevant uncertainties are either directly obtained from the catalogs of the device, or as a result of calibration with more precise devices. In the present study, related to first group, uncertainties of both the volumetric flow rate and temperature were determined after calibration. T-type thermocouples were prepared via a precise thermocouple welding machine; more clearly, cables were turned to thermocouples after welding. Then, the relevant thermocouples were calibrated via a calibration bath (accuracy: ± 0.02 °C). All the thermocouples used in the study were T-type. On the other hand, regarding volumetric flow rate, a measuring cylinder (accuracy: ± 0.2 ml min^{-1}) was utilized for calibration. Other measurements or direct readings were obtained from device-catalogs. It should be stated that all the devices with names/codes/models are explicitly written in Table 1. Details of the devices were also underlined in the recent articles of the authors [29, 30]. For the second group, the common approach introduced by Kline and McClintock [31] was used. Here, the most critical parameter is the two-phase heat transfer coefficient; and therefore, the uncertainty of that parameter was presented separately for each of the heat sink. Uncertainties of derived parameters change based on the experimental conditions, and therefore, for the whole

Table 1 Makes/models of the devices used in the study

Equipment/Device	Make	Model	Remarks
Constant temperature bath	Labo	P200-H22	−20/100 ℃
AC power supply	GW-Instek	APS-7100E	0–1000 VA
Flowmeter	McMillan	S-111	13–100 mL min^{-1}
Manometer	Keller	LEO2	−1/3 bar
Micro-gear pump with digital pump driver	Masterflex/Micropump	75,211–70/73,003–14	36 to 3600 rpm
DC power supply	GW-Instek	GPP-4323	Four channels
Absolute pressure transducer	Omega	PXM01MA0-2.5BARA5T	0–2.5 bar
Differential pressure transducer	Omega	PXM409-350HDWU10V	0–350 mbar
Data logger	Keithley	DAQ6510/7708 multiplexer module	Scanning rate: up to 800 channels/second
Microscope with high-speed camera	Nikon/Fastec	LV-IM/HiSpec 4 Color	up to 298,851 fps
Thermocouple welding machine	Omega	TL-WELD	For welding of the T-type thermocouples

Table 2 Results obtained for uncertainty analysis

Variable/measurement	Results of uncertainty	
Temperature (T)	± 0.1 °C	
Inlet pressure (P_i)	$\pm 0.05\%$ F	
Pressure drop (ΔP)	$\pm 0.08\%$ F	
Heating power (q_{hp})	$\pm 0.6\%$ R	
Volumetric flow rate ($\dot{V}$)	± 0.2 ml min^{-1}	
Mass flux (G)	$\pm 2.69\%$	
Local vapor quality (x_e)	± 1.48–2.46%	
Effective heat flux (q''_{eff})	± 2.85–3.05%	
	CT	**NT**
Heat transfer coefficient (h_{tp})	± 1.71–4.22%	± 2.17–7.55%

F full scale, *R* reading scale

data range an uncertainty-interval including minimum and maximum potential deviations was presented (except mass flux due to very close values.). Numerical values are presented in Table 2. In addition, it should be underlined that results regarding validation of the experimental setup were already presented in our previous article [30].

3 Evaluation of the results and flow physics-based discussion

Within the scope of this experimental study, boiling performance of water flow in a micro-pin fin heat sink having a new type of geometry was investigated, and thermo-hydrodynamic-based physical mechanisms were analyzed through flow visualization. The results and mechanisms were evaluated over comparative approach through conventional micro-pin-finned heat sink. Pure saturated conditions were taken into consideration over the effective heat flux range of 132–272 kW m^{-2}, inlet temperature of approximately 75 °C, and mass flux of 174 kg m^2 s^{-1}. The effective heat flux range corresponds to heating power range of 90 W to 180 W with 10 W steps. The images were gathered at 1000 fps, and left side of any image corresponds to the nearer side the inlet of the heat sink. As stated in the previous section, local pressure was determined via linear interpolation between inlet and outlet pressures, and corresponding saturation temperature was taken into consideration. Saturation temperature determined corresponding to the distance of seventh (outermost) thermocouple from the heat sink inlet ranges approximately between 373.02 and 373.57 K in the present experiments.

3.1 Tests regarding repeatability/reproducibility of the data

Repeatability of the measurements is very important to show the stability, consistency, or reliability of the experimental

results and experimental equipment. In this regard, in Fig. 6a–d, detailed graphs including temperature and pressure measurements were presented for both the heat sinks. Temperature measurements were presented based on readings of the seventh thermocouple (T_{c7}). On the other hand, pressure drop data was presented based on readings of differential pressure transducer. As seen from the graphs, there is a high consistency between the results of the experiments conducted at different date for the same conditions. The results can be presented via quantitative data as follows: For CT, regarding temperature measurements (see Fig. 6a), minimum and maximum absolute differences between two corresponding data of different experiments are 0.004 K and 0.364 K, respectively. The results can be presented as percentage value. The maximum difference corresponds to 0.096%. Regarding pressure drop, for CT (see Fig. 6b), average difference of two corresponding data of different experiments is 1.1% based on the whole database. On the other hand, For NT, regarding temperature measurements (see Fig. 6c), minimum and maximum absolute differences between two corresponding data of different experiments are 0.02 K and 0.52 K, respectively. The results can be presented as percentage value. The maximum difference corresponds to 0.14%. Regarding pressure drop, for NT (see Fig. 6d), average difference of two corresponding data of different experiments is 7.9% based on the whole database. As seen from the results, despite complex thermo-hydrodynamic nature of flow boiling in microchannels, high consistency was obtained for repeability tests.

3.2 Boiling curves

In any boiling study, the first step is to obtain boiling curves; such that, the boiling curves summarize cooling performance of a heat sink, or in other words, they are among the most important performance indicators. In this regard, the boiling curve showing the relation between wall superheat ($\Delta T_{sat} = T_w - T_{sat}$) and effective heat flux is presented in Fig. 7. First data point corresponds to heating power (q_{hp}) of 90 W, and each data point corresponds to the 10 W higher value compared to the previous one. As compatible with the characteristics of saturation region, for both heat sinks, wall superheat increases with increase in effective heat flux. However, the novel heat sink (NT) presents much higher thermal performance. The wall superheat of NT changes from 1.49 to 5.45 °C for the whole heating power range. On the other hand, the wall superheat of CT changes from 2.69 to 7.17 °C in the same range. Under same heat load, the NT keeps the heating surface at lower temperature, which means that the heat transfer mechanism in NT is more effective than that in CT. After the fourth data point corresponding to 120 W, the slope of data distribution of NT relatively decreases compared to the previous data. As stated by Deng
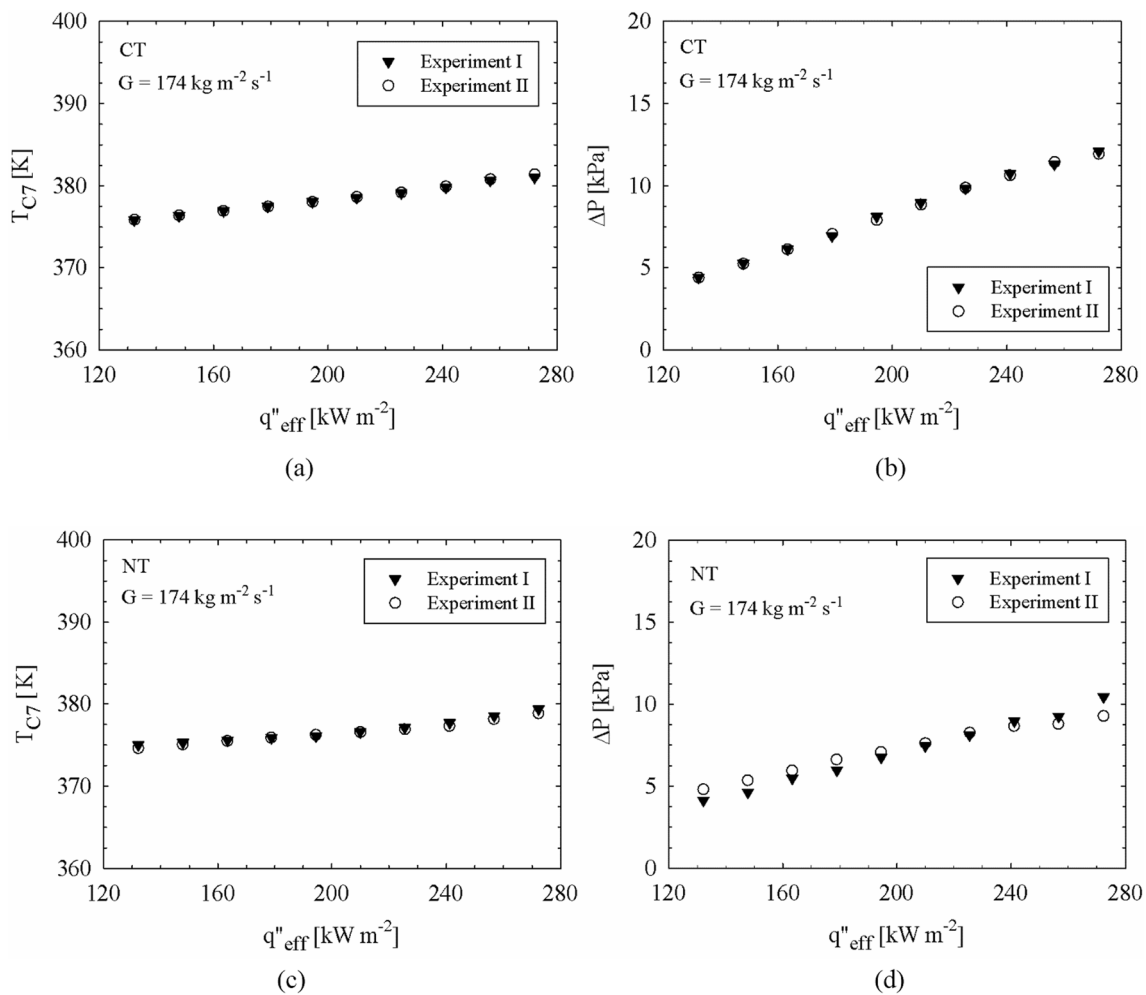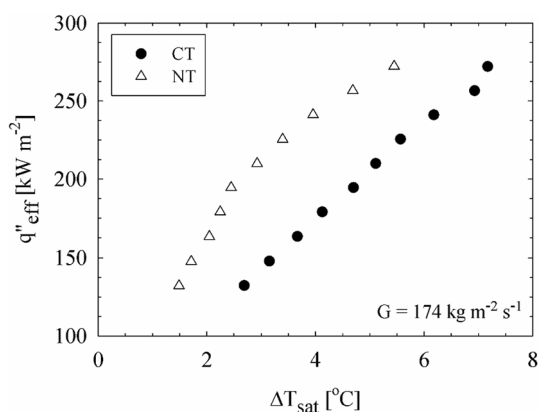
Fig. 6 Repeatability/reproducibility tests

Fig. 7 Relation between effective heat flux and wall superheat: boiling curves

et al. [27], any decrease in the slope of boiling curve means weakening of heat transfer mechanism. However, for the

whole data range, boiling curve of NT is at the left side of CT, in other words, NT presents higher thermal performance for the whole experimental range.

3.3 Analysis of heat transfer coefficient for saturated conditions

Heat transfer coefficients obtained for both the heat sinks at saturated conditions are comparatively presented in Fig. 8a, b. In Fig. 8a, the results are given with variation of effective heat flux, while in Fig. 8b, they are given with variation of local vapor quality. The heat sink coded with NT presents higher heat transfer coefficients than the CT for the whole experimental range. Enhancement ratio ranges from 33.3 to 94.5%, and the average value is 71.6%. Regarding trend of the data distribution, it can be stated that with increase in heat flux or vapor quality, heat transfer coefficients monotonically decrease for both the heat sinks. However, the rate of decrease is more obvious for NT. Based on the first and
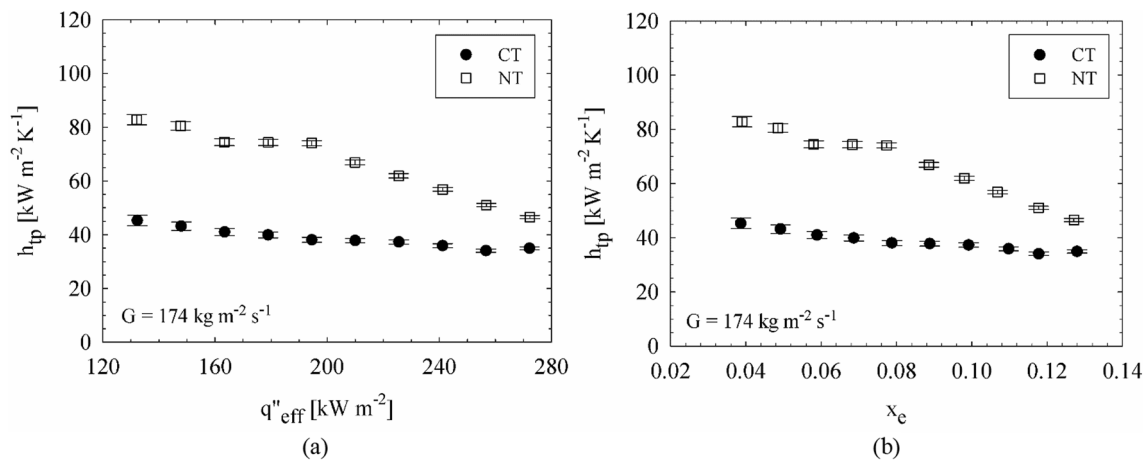
Fig. 8 Heat transfer coefficients obtained for heat sinks at saturated conditions

last data, ratio of decrease is 43.8% for NT, while 22.9% for CT. At medium to high heat fluxes (approximately greater than 195 kW m^{-2}; corresponding to 130 W), rate of decrease in h_{tp} increases for NT compared to lower heat fluxes. On the other hand, local vapor quality for both heat sinks almost linearly increases with heat flux. This result is an expected result, and it is compatible with Eq. (13). It should be stated that error bars were also added to the data points in Fig. 8. As it is clearly seen from the relevant figure the clearance between the horizontal lines of error bars approximately corresponds to symbol size, or even smaller than symbol size. In other words, error bars of different heat sinks are not overlap or intersects, which underlines that there is absolute difference between the results obtained for heat sinks. Reasons of all these results were deeply discussed with scrutinizing of underlying flow mechanism through flow images in following paragraphs.

In the conventional micro-pin-finned heat sink (coded as CT), there is quasi-periodical flow behavior; such that, vapor clusters formed by either growing of a single vapor under highly saturated conditions or coalescing of different bubbles covers relatively large regions. Then, rewetting liquid forces the relevant vapor cluster to move forward or breaks up it. In Fig. 9a–c, an example was given for quasi-periodic behavior takes nearly 67 ms. However, it should be underlined that there is not an exact periodic flow, time and flow patterns change randomly depending on applied heating power or interactions between liquid and vapor components in neighboring locations. Here, the key point is that when a zone on heat transfer surface is covered by vapor, the fins are surrounded by liquid films. This is clearly seen in Fig. 9a, in the figures black lines mean interface between liquid and vapor. The fin surfaces are wet by liquid even if vapor covers the surface. Therefore, evaporation of thin liquid film plays an important role in heat transfer

mechanism of CT. In addition, sharp corners or edges of the fins supports bubble nucleation (see Fig. 9d–f), and lead to deformation of vapor bubbles as seen in Fig. 9d. Deformation of bubbles and enhancement in interactions of liquid and vapor components lead improvement in mixing and play positive role in heat transfer. However, despite existence of alternative ways and above-mentioned advantages of micro-pins, uniform pin distribution suffers bubble blockage problem even at relatively low heating powers. The series of images representing by Fig. 9a–c are examples for bubble blockage. As seen in Fig. 9a, vapor covers a region of heat transfer surface during a period, which means degradation in heat transfer due to relatively low heat transfer coefficient regarding the vapor flow. Breaking of the bubbles by the fins is an advantage; however, due to uniform gaps at each direction, residence time of vapor bubbles on the surface increases. More clearly, for example as seen in Fig. 9f, it is seen that the bubble grows in lateral direction; and which leads increase in waiting period of vapor on heating surface. As concluded, regarding CT, at relatively low heating powers or vapor qualities, both nucleate boiling and thin film evaporation are important heat transfer mechanisms; and fins contribute to heat transfer by deforming bubbles and enhancing mixing of the flow. Also, because the rewetting liquid sweeps the surface, micro-convection with evaporation is other factor playing role in heat transfer. On the other hand, bubble blockage and relevant with this, longer waiting periods of vapor on heating surface are main physical factors leading relatively lower heat transfer coefficient for CT compared to NT.

Increasing heating power leads to intensify of vaporization, and active nucleation loses its effectiveness, or bubble population is significantly diminished. Explosive boiling occurs; such that a bubble nucleated near the edge of a fin suddenly grows and coalescences with bubble clusters.
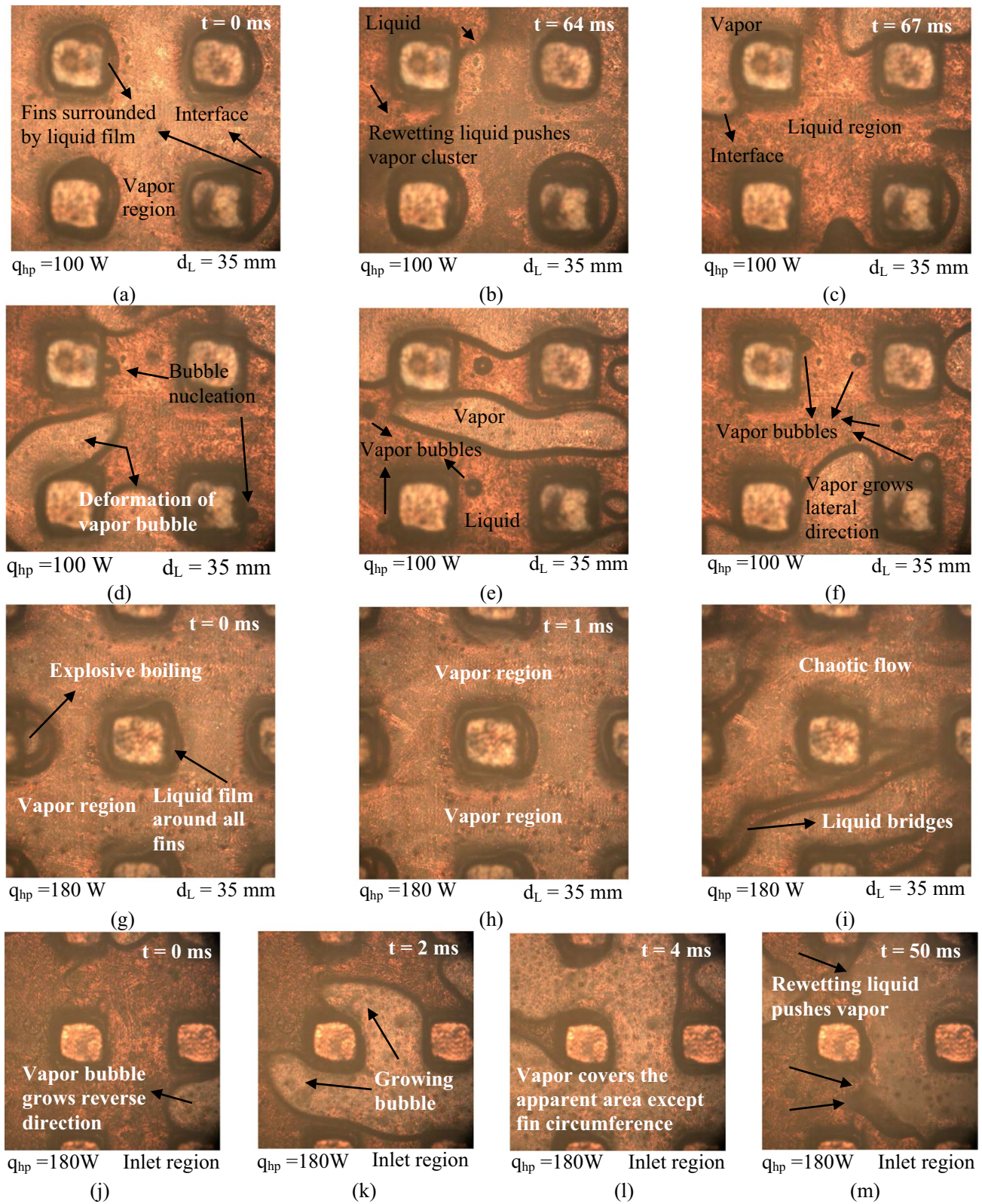
Fig. 9 Flow images representing characteristic flow structure of CT at different operational conditions

Figure 9g, h presented as a time series shows above-mentioned phenomena. Both in Fig. 9g, h, vapor covers all the area captured by the camera, and the bubble nucleating at the edge of the fin (see Fig. 8g) grows in only 1 ms and coalescences with vapor region. Due to explosive boiling and existence of large vapor regions, the heating surface cannot effectively be wetted by rewetting liquid; and therefore, heat transfer deteriorates. As seen in Fig. 9i, decreasing liquid content appears as liquid bridges, or circumferential lines around the fins. Therefore, thin film evaporation and existence of liquid bridges prevent occurrence of critical heat flux (CHF) even at the highest heating power of the present paper (180 W). The strength of the bubble blockage phenomenon regarding CT is presented in Fig. 9j–m as a time series. Relevant images were taken at the heat sink inlet. In the images (Fig. 9j–m), reverse motion of expanding bubble is clearly seen for relatively long time as 50 ms. As concluded, with increase in heating power, regarding CT, micro-convection induced by high bubble population and active nucleate boiling are suppressed; and therefore, these two mechanisms loss their effectiveness on heat transfer. Dominant heat transfer mechanism is thin film evaporation, and liquid bridges and mixing of flow contributes to heat transfer, too. Bubble blockage is the main underlying physical factor for decrease of thermal performance, and this phenomenon strengths with increase in heating power. Intense bubble blockage locally inhibits entering of rewetting liquid to flow passages for variable periods. Also, it should be noted that bubble blockage induces degradation of multiple nucleation or suppression of high bubble population. Therefore, heat transfer coefficients of CT are lower compared to NT, and heat transfer coefficients decrease with increase in heat flux.

For the novel heat sink (NT), flow structure changes depending on geometrical differences. In Fig. 10a–i, various images representing characteristic flow features of NT at relatively low heating powers such as 100 W are shown. In this regard, the images in Fig. 10a–c are presented as a time series. The region in the relevant figures corresponds to expanding section in *"Transition Region-2"* shown in Fig. 4. As seen in Fig. 10a vapor covers the relevant region taken by the camera; however, the fins are surrounded by liquid film, and thus, evaporation of thin film is one of the dominant heat transfer mechanisms for NT. Different from CT, due to existence of larger flow passages, and thus lower-resistant regions, blockage problem is solved; and rewetting liquid pushes vapor toward larger section in a very short time. For example, for the present case, it only takes nearly 7 ms (see Fig. 10c). Therefore, compared to CT, decreasing waiting time of vapor on heat transfer surface is one of the reasons for better thermal performance of NT. On the other hand, as seen in Fig. 10d, e (time series), staggered layout of fins improves breakup process of vapor bubbles. Vapor bubbles

passing between two neighboring channels hit the fin located on the centerline of relevant flow passage. It should be stated that in the present paper the staggered structure was designed in a novel form, more clearly, an area-based staggered distribution was constituted for the first time (see Fig. 4). In each region, fins were organized in inline form; however, different sections were organized as staggered form according to each other. Thus, regional deformation was provided. The reason is expressed as follows: In some previous studies such as Deng et al. [13], it was reported that conventional staggered distribution deteriorated both heat transfer and pressure drop compared to inline type. In this regard, as compatible with the literature, in the present study it is shown that longer waiting or staying time of vapor on heat transfer surface, and relevant this, blockage problem of vapor clusters in the flow passages are among the main influential factors deteriorating thermal performance. In this regard, although breakup of vapor bubbles or better mixing of the flow are useful sides of staggered distribution, conventional staggered form is prone to lead blockage problem and increase in staying time of bubble clusters on surface; and thus, it suppresses advantages of mixing and breakup processes. On the other hand, the novel configuration in the present paper resolves the negative sides of conventional staggered distributions, and thus, provide to benefit from potential of advantages of staggered configuration of fins. Orientation of a vapor bubble toward larger flow section is seen in Fig. 10f. Regional enlargement in flow passages provides lower-resistant ways for bubbles; and thus, blockage is prevented. In addition to prevention of bubble blockage problem, this orientation leads also some other physical phenomena. Low-resistant-flow-passages behave as if they were suction lines, and accelerating flow drags relatively smaller bubbles toward outlet, too. Dragged and/or nucleated vapor bubbles are seen in Fig. 10g–i. Also, in Fig. 10d, e, bubble nucleating at the fin is seen. Therefore, at relatively low heating powers, for NT, nucleate boiling, and micro-convection induced by dragged bubbles play effective role on heat transfer enhancement. As concluded, at relatively low heating powers, regarding NT, evaporation of thin liquid film, nucleate boiling, micro-convection induced by dragged bubbles, and evaporation of rewetting fluid are effective heat transfer mechanisms. Compared to CT, breakup of the vapor bubbles is improved, due to existence of larger flow passages blockage problem is solved and waiting time of vapor on heat transfer surface decreases. Accelerating flow enhances micro-convection and rewetting processes. Therefore, compared to CT, better thermal performance is obtained for NT.

At relatively high heating powers, various images representing characteristic flow features of NT are shown in Fig. 11a–i. The region in Fig. 11a, b corresponds to expanding section in *"Transition Region-2"*. Similar to the cases with relatively low heating power, as seen in Fig. 11a,
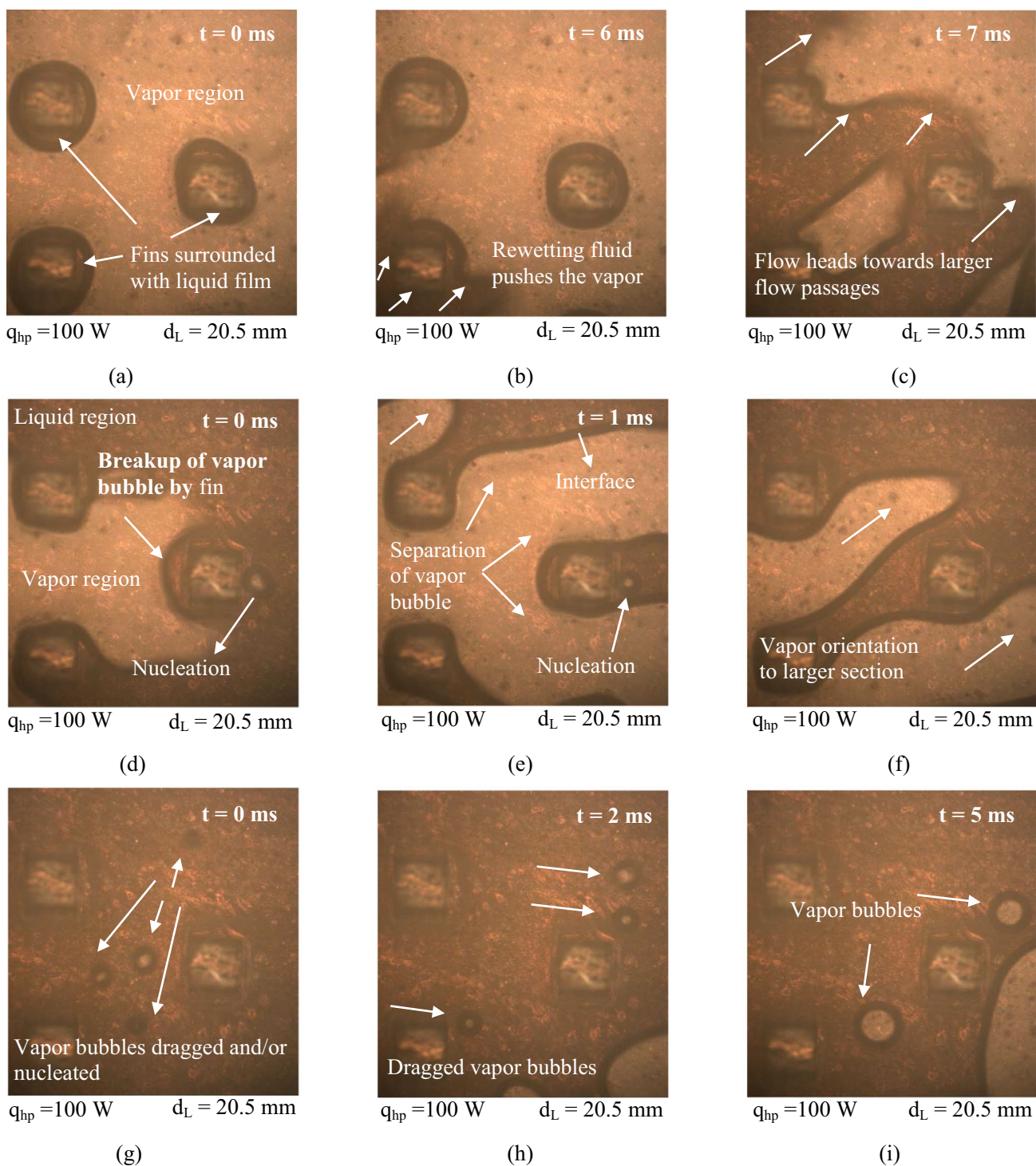
Fig. 10 Flow images representing characteristic flow structure of NT at relatively low heating powers

growing and/or moving vapor orients toward larger flow passages. Also, breakup of vapor, existence of smaller vapor bubbles (Fig. 11a), and enlargement of vapor toward lower-resistant-region (Fig. 11b) are ongoing flow phenomena at high heat loads. Figure 11c corresponds to a region near

centerline of heat sink in *Transition Region-2*. As seen in relevant figure, staggered form deforms vapor bubbles and enhances mixing of flow. However, as a result of increasing heating powers, and thus, increasing heat fluxes, nucleation loses its efficiency on heat transfer. Therefore, at high
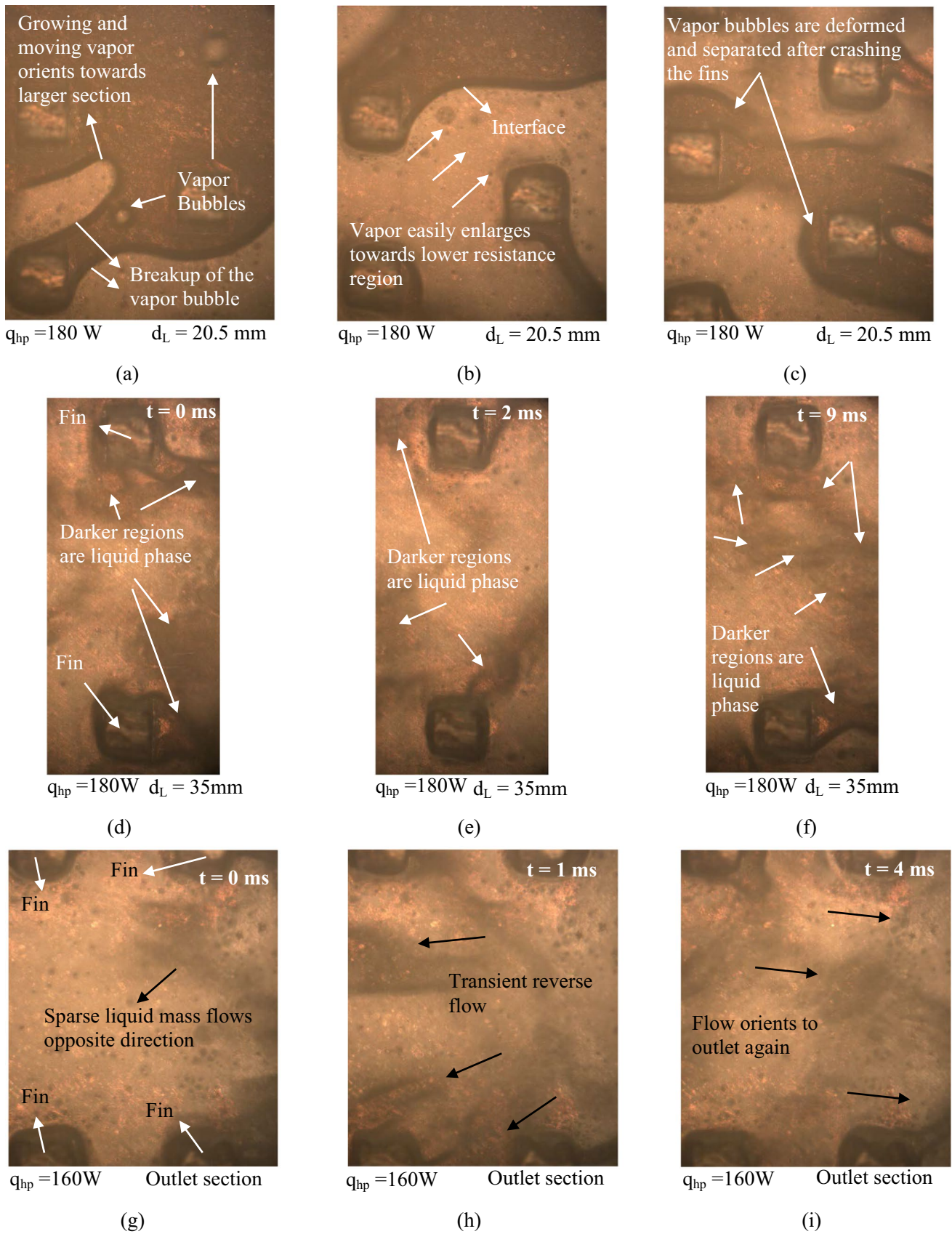
(a) Growing and moving vapor orients towards larger section; Vapor Bubbles; Breakup of the vapor bubble. q_{hp} =180 W, d_L = 20.5 mm

(b) Interface; Vapor easily enlarges towards lower resistance region. q_{hp} =180 W, d_L = 20.5 mm

(c) Vapor bubbles are deformed and separated after crashing the fins. q_{hp} =180 W, d_L = 20.5 mm

(d) Fin; Darker regions are liquid phase; Fin. t = 0 ms. q_{hp} =180W, d_L = 35mm

(e) Darker regions are liquid phase. t = 2 ms. q_{hp} =180W, d_L = 35mm

(f) Darker regions are liquid phase. t = 9 ms. q_{hp} =180W, d_L = 35mm

(g) Fin; Fin; Sparse liquid mass flows opposite direction; Fin; Fin; Outlet section. t = 0 ms. q_{hp} =160W

(h) Transient reverse flow; Outlet section. t = 1 ms. q_{hp} =160W

(i) Flow orients to outlet again; Outlet section. t = 4 ms. q_{hp} =160W

Fig. 11 Flow images representing characteristic flow structure of NT at relatively high heating powers

heat fluxes, thin liquid film evaporation, flow mixing-based micro-convection, and accelerating flow-based enhanced convective flow boiling characteristics are dominant heat transfer mechanisms. In brief, convective flow boiling covering all the above-mentioned flow phenomena is the dominant heat transfer mechanism. Figure 11d–f corresponds to a zone in "Region-4" (see Fig. 4). There is a continuous forward flow; and this is named as vapor–liquid complex flow in which vapor flows with sparse liquid mass in chaotic form. Evaporation of liquid in the vapor–liquid complex flow is the effective physical phenomenon influencing thermal characteristics. In Fig. 11g–i, one of the important flow phenomena is presented. As also underlined in the previous sections, rate of decrease of two-phase heat transfer coefficients of NT increases at medium to high heat fluxes compared to lower heat fluxes. The reason is the decreasing resistance of the heat sink against reverse flow motions at the outlet section due to decreasing fin number. Reverse flow motions at the outlet stem from flow fluctuations, and absent of enough resistance at fields near outlet induces partial reverse motions. In this regard, in the relevant figures presented as a time series (Fig. 11g–i), only for 3 ms, reverse bulk motion is seen, then at the fourth milliseconds, flow again orients to outlet. This transient reverse flow is the reason of increasing rate of decrease of heat transfer coefficient of NT. As concluded, at relatively high heat fluxes, regarding NT, convective flow boiling mechanisms including thin liquid film evaporation, flow mixing-based micro-convection, accelerating flow and evaporation of liquid in the vapor–liquid complex flow are dominant heat transfer mechanisms. Due to more effective convective boiling characteristics, the NT presents better thermal performance than CT. However, due to few fin numbers at the heat sink outlet, resistance of heat sink against reverse flow motions decreases and transient reverse flow occurs. Due to transient reverse flow, decrease rate of heat transfer coefficient of NT increases compared to

relatively low heat flux cases. However, it should be stated that, for the whole data range, NT shows better thermal performance than CT.

3.4 Analysis of pressure drop

In Fig. 12a, b, pressure drops obtained for both the heat sinks are presented, respectively, based on effective heat flux (Fig. 12a) and vapor quality (Fig. 12b). As clearly explained in Sect. 2.3, the pressure drop term (ΔP) can be evaluated as equal with the two-phase pressure drop (or the pressure drop throughout the heat sink). As an expected result, for both the NT and CT, pressure drop linearly increases with effective heat flux or vapor quality. The reason is related to increasing vapor content and increasing difference between superficial velocities of liquid phase and vapor phase. As a result, with increase in heat flux, both two-phase pressure drop components named as frictional and acceleration pressure drops, and thus, two-phase pressure drop increase. In the literature [17, 25], similar relation between pressure drop and heat flux was also reported. Here, the important point is that discussion should be performed through comparative results of NT and CT. In addition to thermal success, NT also presents much lower pressure drop than CT. Compared to CT, for the whole dataset, NT presents lower pressure drop up to 18.3% (and as average up to 14.2%). Generally, enhancement of heat transfer leads undesirable results for pressure drop; contrary to this, NT both improves thermal performance and reduces pressure drop, and thus, pumping power requirements. The basic physical reason is the prevention of bubble blockage problem due to enlarging flow passages in the main flow direction. Decreasing resistance against flow enables the fluid to easily pass the flow passages. Bubbles blocked in the flow passages enlarge at all directions under heating power and apply a force called as evaporation momentum force [32, 33]. The evaporation momentum force having
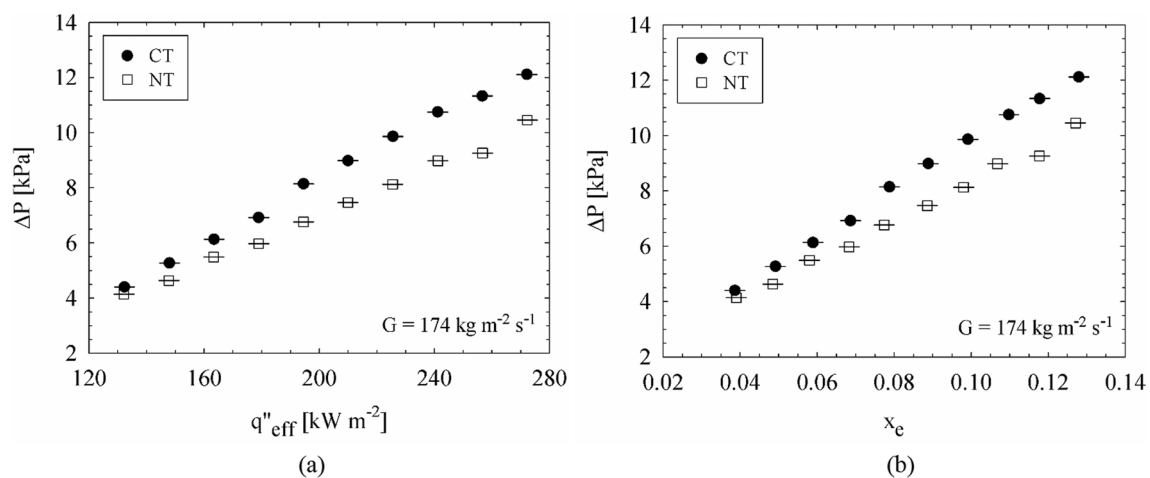

Fig. 12 Pressure drops obtained for heat sinks

an impact in reverse direction, in other words, toward the heat sink inlet induces two main problems: (1) flow reversal occurs, and (2) arrival of rewetting fluid to flow passages is getting hard or inhibited for a while. Therefore, both the existence of more fins in the flow passages and the additional resistance applied by evaporation momentum force against liquid inertia force (regarding rewetting fluid) are the main underlying reasons to being obtained relatively high pressure drops for CT compared to NT. It should be noted that error bars were also added to the data points in Fig. 12. As it is clearly seen from the relevant figure, the clearance between the horizontal lines of error bars is quite small. Two lines are seen as if there was a single line. This result proves the certain difference of results of two heat sinks.

3.5 Analysis of instabilities

Fluctuations of inlet pressure and temperature are strong indicators for the level of flow boiling instabilities. In this regard, in transient manner, Fig. 13a–d are presented to show instability results of CT and NT at various operational conditions. Figure 13a, b represents inlet temperature

fluctuations, respectively, at relatively low and high heating powers. At both heating cases, more stable temperature readings are obtained for NT. As quantitative results, at the heating power of 100W, the maximum and average deviations between two consecutive data of NT are ± 0.22 °C and ± 0.07 °C, respectively. On the other hand, the maximum and average deviations are, respectively, ± 0.6 °C and ± 0.17 °C for CT. At high heating power (180 W), the maximum and average deviations between two consecutive data of NT are ± 0.26 °C and ± 0.07 °C, respectively. On the other hand, the maximum and average deviations are, respectively, ± 0.7 °C and ± 0.25 °C for CT. Also, according to the standard deviation equation presented by Deng et al. [13], deviations for NT at both the 100 W and 180 W are approximately ± 0.08 °C. On the other hand, in this regard, deviations for CT at 100 W and 180 W are ± 0.16 °C and ± 0.23 °C, respectively.

Regarding inlet pressure fluctuations, again, NT has advantageous compared to CT. At the heating power of 100 W, the maximum and average deviations between two consecutive data of NT are ± 0.43 kPa and ± 0.11 kPa, respectively. Similarly, for 180 W, maximum and average
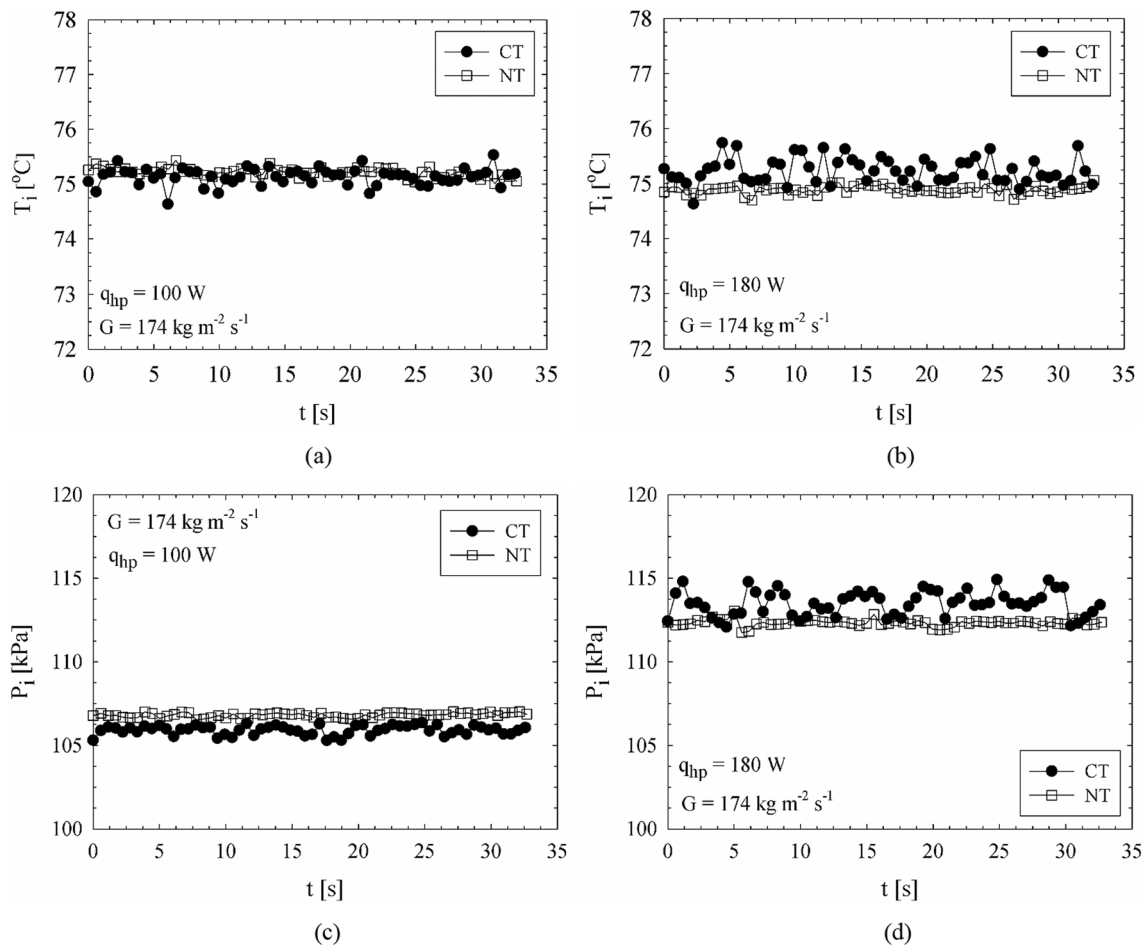

Fig. 13 Instability results of CT and NT at various operational conditions

deviations for NT are ± 1.3 kPa and ± 0.16 kPa, respectively. On the other hand, for CT, the maximum and average deviations between two consecutive data are ± 0.99 kPa and ± 0.28 kPa at 100 W; and these values are ± 2.30 kPa and ± 0.59 kPa at 180 W, respectively. According to standard deviation equation, deviations for NT at the 100 W and 180 W are approximately ± 0.13 kPa and ± 0.21 kPa, respectively. On the other hand, deviations for CT at 100 W and 180 W are ± 0.28 kPa and ± 0.75 kPa, respectively.

As concluded, CT shows clearly higher fluctuations than NT regarding both inlet temperature and pressure. The underlying reasons are the strong effect of bubble blockage and interactions between evaporation momentum force and liquid inertia force. Liquid inertia force is applied by the rewetting or refreshing fluid entering the heat sink, and it is necessary for forward motion of flow, while evaporation momentum force is applied by blocked and/or confined vapor clusters and it also impacts toward inlet of the heat sink. Interactions of these two forces induce pressure fluctuations. Especially, near the heat sink inlet, if there is a reversal flow, vapor phase interacts with the liquid in the inlet plenum, and high magnitude temperature fluctuations occur.

4 Conclusions

Combined influence of regional staggered pin fin arrangement and regional cross-sectional enlargement on thermo-hydrodynamic characteristics of flow boiling in micro-pin fin heat sinks was experimentally investigated. Physical mechanisms were analyzed through flow visualization; and the results obtained for the novel heat sink was evaluated comparatively with conventional micro-pin fin heat sinks. Details have been presented in previous sections; here some important remarks have been briefly underlined:

- For both the NT and CT, wall superheat increases with increase in effective heat flux. However, NT presents much higher thermal performance. The wall superheat of NT changes from 1.49 to 5.45 °C for the whole heating power range. On the other hand, the wall superheat of CT changes from 2.69 °C to 7.17 °C in the same range. These results physically mean that the NT can keep the heating surface at lower temperature for the same heat load.
- The NT presents higher heat transfer coefficients than CT for the whole experimental range. Enhancement ratio ranges from 33.3 to 94.5%, and the average value is 71.6%. With increase in vapor quality or heat flux, heat transfer coefficients monotonically decrease for both heat sinks. However, rate of decrease is more obvious for NT.

- Regarding CT, important heat transfer mechanisms are reported as thin film evaporation and nucleate boiling at relatively low heating powers or vapor qualities. Fins deform bubbles and enhance mixing of flow, thus, contribute to heat transfer. Also, micro-convection with evaporation is other factor playing role in heat transfer since rewetting liquid sweeps the surface. On the other hand, bubble blockage and relevant with this, longer waiting period of vapor on heating surface are main physical factors leading relatively lower heat transfer coefficient of CT compared to NT.
- With increase in heating power, regarding CT, micro-convection induced by high bubble population and nucleate boiling are suppressed, and thus, these two mechanisms loss their effectiveness on heat transfer. Dominant heat transfer mechanism is thin film evaporation. Also, liquid bridges and mixing of flow contribute to heat transfer. Bubble blockage is the main underlying physical factor for decreasing thermal performance, and bubble blockage becomes violent with increase in heating power.
- Regarding NT, for relatively low heat loads, nucleate boiling, evaporation of thin liquid film, micro-convection induced by dragged bubbles, and evaporation of rewetting fluid are effective heat transfer mechanisms. Compared to CT, breakup of vapor bubbles is improved, due to existence of larger flow passages blockage problem is solved and vapor-waiting time on heat transfer surface decreases. Accelerating flow enhances micro-convection and rewetting processes. Therefore, compared to CT, better thermal performance is obtained for NT.
- At relatively high heat fluxes, regarding NT, convective flow boiling mechanisms including thin liquid film evaporation, flow mixing-based micro-convection, accelerating flow and evaporation of liquid in the vapor–liquid complex flow are dominant heat transfer mechanisms. Due to more effective convective boiling characteristics, the NT presents better thermal performance than CT. However, due to few fin numbers at the heat sink outlet, heat sink resistance against reverse flow motions decreases and transient reverse flow occurs. Due to transient reverse flow, decrease rate of heat transfer coefficient of NT increases compared to relatively low heat flux cases.
- For both the NT and CT, there is a linear relationship between pressure drop and effective heat flux or vapor quality; and increasing heat flux or vapor quality increases two-phase pressure drop.
- In addition to thermal success, NT also presents much lower pressure drop than CT. Compared to CT, for the whole dataset, NT presents lower pressure drop up to 18.3% (and as average up to 14.2%).
- At both the low and high heat fluxes, the NT successfully suppresses both the temperature and pressure instabili-

ties. Compared to CT, the NT presents lower inlet pressure fluctuations and inlet temperature fluctuations.

- In follow-up studies, as a suggestion, critical heat flux condition of this type of heat sinks can be correlated with mass flux.

Declarations

Conflict of interest There is no conflict of interest. All authors of present paper declared this statement.

References

1. Karayiannis TG, Mahmoud MM (2017) Flow boiling in microchannels: fundamentals and applications. Appl Therm Eng 115:1372–1397. https://doi.org/10.1016/j.applthermaleng.2016.08.063

2. Markal B, Aydin O, Avci M (2012) Exergy analysis of a counterflow Ranque-Hilsch vortex tube having different helical vortex generators. Int J Exergy 10:228–238. https://doi.org/10.1504/IJEX.2012.045867

3. Nuntadusit C, Wae-hayee M, Kaewchoothong N (2018) Heat transfer enhancement on a surface of impinging jet by increasing entrainment using air-augmented duct. Int J Heat Mass Transf 127:751–767. https://doi.org/10.1016/j.ijheatmasstransfer.2018.06.130

4. Markal B (2019) The effect of total flowrate on the cooling performance of swirling coaxial impinging jets. Heat Mass Transf und Stoffuebertragung 55:3275–3288. https://doi.org/10.1007/s00231-019-02653-7

5. Gupta NK, Sharma A, Rathore PKS, Verma SK (2020) Thermal performance optimization of heat pipe using nanofluid: response surface methodology. J Braz Soc Mech Sci Eng 42:590. https://doi.org/10.1007/s40430-020-02668-w

6. Domiciano KG, Krambeck L, Flórez JPM, Mantelli MBH (2022) Thin diffusion bonded flat loop heat pipes for electronics: fabrication, modelling and testing. Energy Convers Manag. https://doi.org/10.1016/j.enconman.2022.115329

7. Lee PC, Pan C (2008) Boiling heat transfer and two-phase flow of water in a single shallow microchannel with a uniform or diverging cross section. J Micromech Microeng. https://doi.org/10.1088/0960-1317/18/2/025005

8. Lu CT, Pan C (2008) Stabilization of flow boiling in microchannel heat sinks with a diverging cross-section design. J Micromech Microeng. https://doi.org/10.1088/0960-1317/18/7/075035

9. Lu CT, Pan C (2011) Convective boiling in a parallel microchannel heat sink with a diverging cross section and artificial nucleation sites. Exp Therm Fluid Sci 35:810–815. https://doi.org/10.1016/j.expthermflusci.2010.08.018

10. Fu BR, Tsou MS, Pan C (2012) Boiling heat transfer and critical heat flux of ethanol-water mixtures flowing through a diverging microchannel with artificial cavities. Int J Heat Mass Transf 55:1807–1814. https://doi.org/10.1016/j.ijheatmasstransfer.2011.11.051

11. Fu BR, Lin PH, Tsou MS, Pan C (2012) Flow pattern maps and transition criteria for flow boiling of binary mixtures in a diverging microchannel. Int J Heat Mass Transf 55:1754–1763. https://doi.org/10.1016/j.ijheatmasstransfer.2011.11.030

12. Wan W, Deng D, Huang Q et al (2017) Experimental study and optimization of pin fin shapes in flow boiling of micro pin fin heat sinks. Appl Therm Eng 114:436–449. https://doi.org/10.1016/j.applthermaleng.2016.11.182

13. Deng D, Zeng L, Sun W et al (2021) Experimental study of flow boiling performance of open-ring pin fin microchannels. Int J Heat Mass Transf 167:120829. https://doi.org/10.1016/j.ijheatmasstransfer.2020.120829

14. Lie YM, Ke JH, Chang WR et al (2007) Saturated flow boiling heat transfer and associated bubble characteristics of FC-72 on a heated micro-pin-finned silicon chip. Int J Heat Mass Transf 50:3862–3876. https://doi.org/10.1016/j.ijheatmasstransfer.2007.02.010

15. Krishnamurthy S, Peles Y (2008) Flow boiling of water in a circular staggered micro-pin fin heat sink. Int J Heat Mass Transf 51:1349–1364. https://doi.org/10.1016/j.ijheatmasstransfer.2007.11.026

16. Ma A, Wei J, Yuan M, Fang J (2009) Enhanced flow boiling heat transfer of FC-72 on micro-pin-finned surfaces. Int J Heat Mass Transf 52:2925–2931. https://doi.org/10.1016/j.ijheatmasstransfer.2009.02.031

17. Qu W, Siu-Ho A (2009) Experimental study of saturated flow boiling heat transfer in an array of staggered micro-pin-fins. Int J Heat Mass Transf 52:1853–1863. https://doi.org/10.1016/j.ijheatmasstransfer.2008.10.008

18. Law M, Lee PS (2015) A comparative study of experimental flow boiling heat transfer and pressure characteristics in straight- and oblique-finned microchannels. Int J Heat Mass Transf 85:797–810. https://doi.org/10.1016/j.ijheatmasstransfer.2015.01.137

19. Law M, Lee PS (2016) Effects of varying secondary channel widths on flow boiling heat transfer and pressure characteristics in oblique-finned microchannels. Int J Heat Mass Transf 101:313–326. https://doi.org/10.1016/j.ijheatmasstransfer.2016.05.055

20. Deng D, Chen L, Wan W et al (2019) Flow boiling performance in pin fin- interconnected reentrant microchannels heat sink in different operational conditions. Appl Therm Eng 150:1260–1272. https://doi.org/10.1016/j.applthermaleng.2019.01.092

21. Chien LH, Liao WR, Ghalambaz M, Yan WM (2019) Experimental study on convective boiling of micro-pin-finned channels with parallel arrangement fins for FC-72 dielectric fluid. Int J Heat Mass Transf 138:390–400. https://doi.org/10.1016/j.ijheatmasstransfer.2019.04.072

22. Qin L, Li S, Zhao X, Zhang X (2021) Experimental research on flow boiling characteristics of micro pin-fin arrays with different hydrophobic coatings. Int Commun Heat Mass Transf 126:105456. https://doi.org/10.1016/j.icheatmasstransfer.2021.105456

23. Lee PS, Garimella SV (2008) Saturated flow boiling heat transfer and pressure drop in silicon microchannel arrays. Int J Heat Mass Transf 51:789–806. https://doi.org/10.1016/j.ijheatmasstransfer.2007.04.019

24. Cui P, Liu Z (2023) Experimental study on flow boiling in ultra-high-aspect-ratio copper microchannel heat sink. Appl Therm Eng 223:119975. https://doi.org/10.1016/j.applthermaleng.2023.119975

25. Balasubramanian K, Lee PS, Teo CJ, Chou SK (2013) Flow boiling heat transfer and pressure drop in stepped fin microchannels. Int J Heat Mass Transf 67:234–252. https://doi.org/10.1016/j.ijheatmasstransfer.2013.08.023

26. Law M, Lee PS, Balasubramanian K (2014) Experimental investigation of flow boiling heat transfer in novel oblique-finned microchannels. Int J Heat Mass Transf 76:419–431. https://doi.org/10.1016/j.ijheatmasstransfer.2014.04.045

27. Mirmanto M (2014) Heat transfer coefficient calculated using a linear pressure gradient assumption and measurement for flow boiling in microchannels. Int J Heat Mass Transf 79:269–278. https://doi.org/10.1016/j.ijheatmasstransfer.2014.08.022

28. Deng D, Tang Y, Liang D et al (2014) Flow boiling characteristics in porous heat sink with reentrant microchannels. Int J Heat Mass Transf 70:463–477. https://doi.org/10.1016/j.ijheatmasstransfer.2013.10.057

29. Qu W, Mudawar I (2003) Measurement and prediction of pressure drop in two-phase micro-channel heat sinks. Int J Heat Mass Transf 46:2737–2753. https://doi.org/10.1016/S0017-9310(03)00044-9

30. Markal B, Kul B (2022) Combined influence of artificial nucleation site and expanding cross section on flow boiling performance of micro pin fins. Int Commun Heat Mass Transf 135:106081. https://doi.org/10.1016/j.icheatmasstransfer.2022.106081

31. Markal B, Kul B, Avci M, Varol R (2022) Effect of gradually expanding flow passages on flow boiling of micro pin fin heat sinks. Int J Heat Mass Transf 197:123355. https://doi.org/10.1016/j.ijheatmasstransfer.2022.123355

32. Kline SJ, McClintock FA (1953) Describing uncertainties in single-sample experiments. Mech Eng 75:3–8

33. Kandlikar SG (2004) Heat transfer mechanisms during flow boiling in microchannels. J Heat Transfer 126:8–16. https://doi.org/10.1115/1.1643090

34. Lee HJ, Liu DY, Yao SC (2010) Flow instability of evaporative micro-channels. Int J Heat Mass Transf 53:1740–1749. https://doi.org/10.1016/j.ijheatmasstransfer.2010.01.016